Abbreviation and Acronym
CCD = charge-coupled device

Therefore, we evaluated the safety of this procedure, not only for short time periods to assess hemodynamic changes but also for longer periods to assess chronic complications, including infections, chronic pericarditis, and other life-threatening complications. Among various ready-made endoscopes, adequate types for pericardial endoscopy were selected. To identify the anatomy of the heart, we defined the basic method to steer the endoscope and stabilize the view.

MATERIALS AND METHODS

Surgical Procedure

All experimental protocols were approved by the institutional ethical committee. Studies were performed in 6 mongrel swine weighing 26 to 61 kg. After nitrous oxide inhalation, swine were intubated and ventilated with room air by the constant-volume cycled respirator (Harvard Apparatus model 607; Harvard Appatatus, Hoilliston, Mass) and anesthetized with 1.5% to 2% isoflurane. A fluid-filled cannula was placed in the left carotid artery and connected to the transducer to monitor arterial blood pressure. A great cervical vein cannula was used to infuse normal saline at a rate of 100 to 200 mL/h to replace spontaneous fluid losses and to inject drugs. Electrocardiogram and pulse oxymetry were continuously monitored.

Mechanical irritation of the pericardium may cause Bezold–Jarisch (vagal) reflex and bradycardia that can result in significant deterioration of hemodynamics; therefore, immediately before the pericardiocentesis, 1 mg of atropine was administered to suppress the vagal reflex and an additional 0.5 mg of atropine was administered when the heart rate decreased to less than 70 beats/min. After local anesthesia, an 18G epidural needle connected to a 10-mL syringe filled with contrast material was inserted from the subxyphoid toward the heart shadow under x-ray fluoroscopic guidance.[18] After puncture of the pericardial membrane, the guide wire (outer diameter = 0.81 mm) was inserted into the pericardial space, and the catheter sheath was inserted along the guide wire to the pericardial space. We used 6 types of sheaths. The size, stiffness, shape, and material of each sheath are shown in Figure 1. Sheaths were selected in accordance with the diameter of the endoscope. Six ready-made endoscopes (Olympus Medical Systems Corp, Tokyo, Japan) were used. The model number, visual angle, direction of lens, size, device ports, optical image system, and features of the endoscopes are shown in Figure 2. The endoscopes are advanced through the variety of sheaths, checking the effects of hemodynamic data, controllability, and quality of the view. We tried to maintain a clear view by regulating the amount of air and saline insufflations through the working port of the endoscope. Measured vital signs, fluoroscopic images, and endoscopic images were analyzed and evaluated after each experiment. To assess chronic effects, animals were kept alive for 2 weeks and then inspected for evidence of injuries to pericardium, lungs, and other organs.

RESULTS

Effect of Endoscope and Sheath Size on Hemodynamic Parameters

The performance of the endoscope increases as a function of the diameter of the endoscope; however, the hemodynamics may deteriorate. Thus, the adequate diameter of the endoscope with acceptable visual images without significantly changing the hemodynamics should be determined. Representative hemodynamic data during pericardial endoscopy are shown in Figure 3. The endoscope with the largest diameter (6.9 mm in ES5) did not cause significant deterioration of hemodynamic parameters; thus, the endoscope with a diameter less than 6.9 mm is acceptable.

To obtain a clear image, design of the optomechanical device is important. Mounting a charge-coupled device (CCD) camera on the tip of the endoscope to connect directly to the objective lens significantly improved image quality (Figure 4, *D, F*). However, this is difficult to do with a thinner endoscope because of limitations on the miniaturization of

No	ID(F)	Model	Material	Stiffness	Shape	Check valve	Image
SH1	10	radifocus introducer-IIH	polypropylene	soft	curved	tight	
SH2	15	handmade	polypropylene	soft	straight	tight	
SH3	21	handmade	polytetra-fluoroethylene	floppy	floppy	tight	
SH4	18	capiox percutaneous catheter kit	polypropylene	hard	curved	none	
SH5	16.5	TOLOCKER Ø 5.5mm	stainless	solid	straight	loose	
SH6	33	TOLOCKER Ø 11mm	stainless	solid	straight	loose	

FIGURE 1. List of the sheaths used. Internal diameter in French, model name, material, stiffness, shape of the tip, durability of the check valve, and an image of the sheath (*white scale bars* = 5 cm). *ID*, Internal diameter; *F*, French.

No	Model	Visual angle(°)	Direction of lens(°)	Ø OD(mm)	Device port (Ø mm)	Adequate sheath	CCD on the Tip	Purpose or usage	Image	Performance
ES1	URF-P5	90	0	2.9	1.2	SH1	×	Designed for pyelo-urine tract	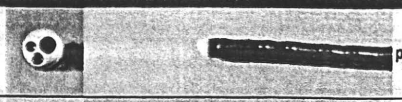	poor
ES2	BF-XP160F	90	0	3.25	1.2	SH1 SH2 SH5	×	Designed for tracho-bronchial tract	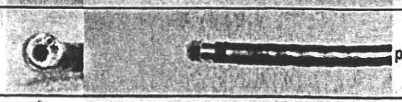	poor
ES3	BF-MP160F	120	0	5.0	2.0	SH2 SH5	×	Designed for tracho-bronchial tract		moderate
ES4	IPLEX FX IV8420	120	90	4.0	non	SH2 SH3 SH4	○	Designed for industrial usage, i.e., to check internal surface of pipes. Robotic controller attached	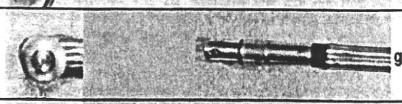	good
ES5	BF TYPE UC160F-OL8	80	35	6.9	2.0	SH3 SH4 SH6	×	Designed for tracho-bronchial tract, with ultrasonic imaging system		well
ES6	GIF-XP150N	120	0	5.5	2.0	SH3 SH4 SH5	○	Designed for trans-nasal gastro-intestine camera	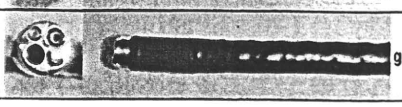	good

FIGURE 2. List of the endoscopes used. Models of the endoscope, visual angle, direction of lens (angle along the longitudinal axis), outer diameter, inner diameter of utility port, adequate sheath, whether CCD camera is mounted on the tip or not, features of the endoscope, images of the endoscope (*scale bars* = 5 mm), and the performance of the endoscope in the pericardial space. *CCD*, Charge-coupled device; *OD*, outer diameter.

the CCD camera. Therefore, the CCD camera was mounted on the body of the thin endoscope and connected to the objective lens by a bundle of flexible optic fibers, which significantly improved image quality (Figure 4, *A–C, E*). Because the thickest endoscope (outer diameter = 6.9 mm) was hemodynamically tolerable, we concluded that mounting the CCD on the endoscope tip was adequate for pericardial endoscopy. Taking these results into account, we selected ES4 and ES6 as adequate for a pericardial endoscope.

The selection of the sheath was more important. To insert a large endoscope into a pericardial space, sheaths with a larger diameter are required, but ready-made larger sheaths are uncommon (SH1, SH5, SH6) and most of them are solid (SH5, SH6). Solid sheaths were unstable in positioning, and use of SH6 sometimes caused significant deterioration of hemodynamic parameters. Therefore, after insertion of the endoscope, withdrawal of the sheath was required to stabilize hemodynamic parameters (Figure 3, *A*). Accordingly, we prepared our handmade flexible sheath with a larger diameter (SH2, SH3, SH4), which did not cause a significant change in hemodynamic parameters (Figure 3, *B*). A check valve on the sheath was also important to maintain the volume of air in the pericardial space. The SH3 exhibited the best performance.

Clear Visualization

Our first achievement was to establish the method to obtain a clear view of the pericardial space by endoscopy. Expansion of the pericardial space by air enables us to maintain a distance from the camera to the heart surface, which is necessary for a clear view. An equal volume of saline was injected in some experiments, but a good image was not obtained and there was significant deterioration of hemodynamic parameters (Figure 3, *B*). Therefore, we decided to inject air to expand the pericardial space.

A larger amount of air infusion provides better vision, but on the other hand it may deteriorate hemodynamic parameters by inhibiting diastolic function of the ventricles. Injection of 100 to 200 mL of gas into the pericardial space caused no hemodynamic changes (±5 mm Hg) and allowed a stable view. In addition, resulting decreases in systolic blood pressure were less than 10 mm Hg, which is almost tolerable.

Orientation of the View

Determination of orientation of the view is important for an endoscopic-guided operation. Because of strong motion artifacts in the visual field, x-ray fluoroscopic guidance is essential to determine orientation of the tip of the endoscope. Furthermore, recognition of several landmarks of the heart can also help in understanding orientation. Infusion of 10 to 20 mL of saline and 50 to 100 mL of air into the pericardial space gives us a clear view of fluid levels. The fluid level is an important compass for horizontal

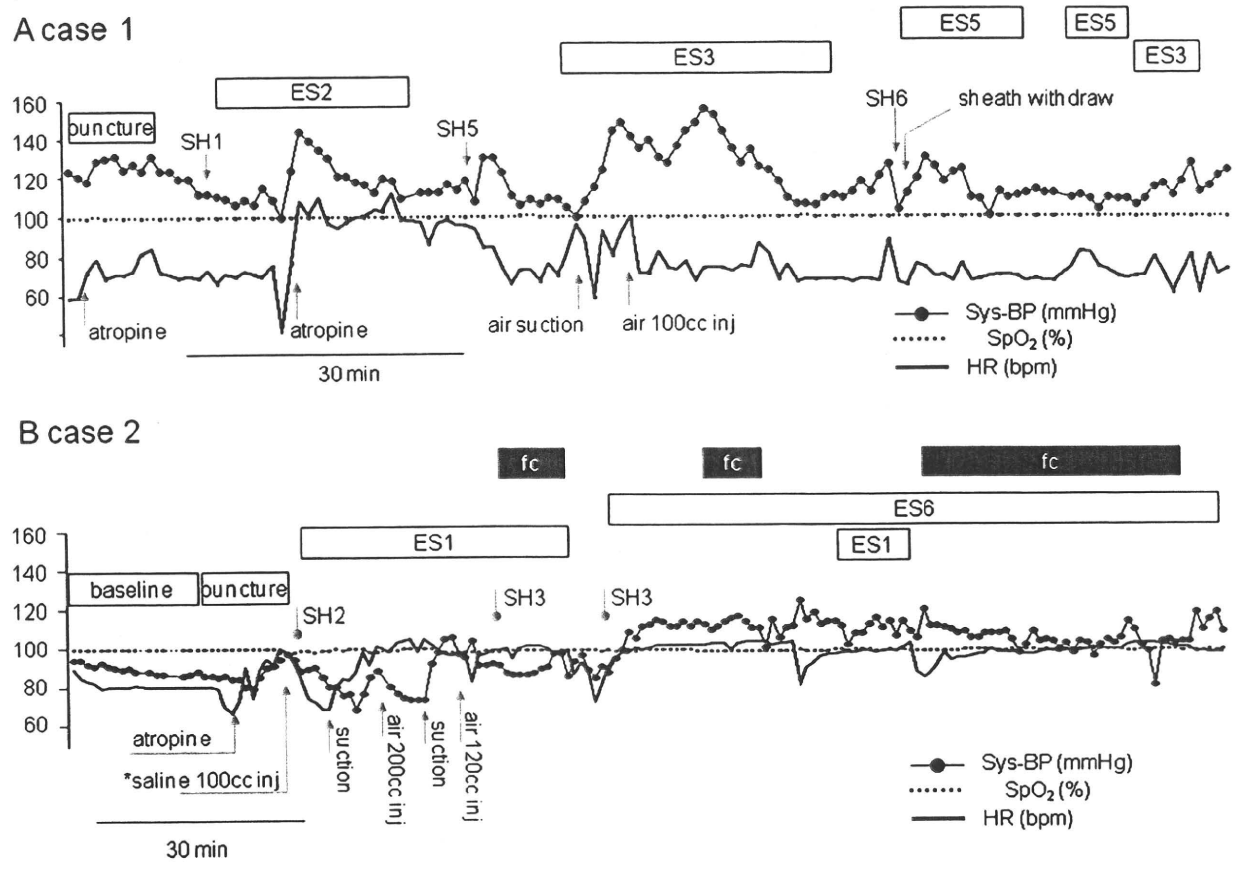

FIGURE 3. Systolic blood pressure, pulse oxymetry, and heart rate as a function of time during procedures of representative cases. *Upper white bars* in the graphs denote period of endoscope insertion, and *black bars* denote insertion of laparoscopic forceps. *Upper gray arrows* denote the time of insertion of each sheath, and *lower gray arrows* denote the timing of administration of atropine, suction, and injection of air/saline into the pericardial space. Hemodynamic parameters during procedure are well within tolerable limits. *Sys-BP*, Systolic blood pressure; SpO_2, pulse oxymetry; *HR*, heart rate; *ES*, endoscope; *fc*, forceps; *SH*, sheath.

direction of the visual field. Landmarks (Figure 5) in the visual field also help us to recognize the position of the tip of the endoscope. Left and right atrial appendages are clear landmarks (Figure 5, *A, C, M, P, Q, S, T, U*). Other heart landmarks, that is, the aortic root (Figure 5, *K*), pulmonary veins (Figure 5, *G, N*), superior vena cava (Figure 5, *E*), and coronary arteries (Figure 4, *A–F*; Figure 5, *R*), also give us a clue to define the orientation. Adjacent organs—the lung, diaphragmatic membrane (Figure 5, *I, W*), and puncture site (Figure 5, *V*)—can be good landmarks.

Control of Endoscopes

It is an advantage to understand the movement of the endoscope to stabilize the tip of the device at the exact location. After the modified Seldinger technique, the anteroapical portion of the pericardium was penetrated by sheaths. By advancing and retracting the endoscope, the tip of the endoscope simply moved forward and backward along the anterior interventricular groove. In this manner, the endoscope was straight, the x-ray showed an "I-shape" configuration, and the heart was observed as in an upward-viewing manner (apex to base direction, Figure 6, *F*). As the endoscope was advanced, the left anterior descending coronary artery (Figure 4, *A, E, F*), left atrial appendage (Figure 4, *E*; Figure 5, *A, M, S, T*), and aortic root were observed (Figure 5, *K*). By bending the endoscopic tip toward the right side, the outflow tract and right ventricle (Figure 5, *O*) were observed; by bending toward the left, the left pulmonary veins could be observed (Figure 5, *G*). However, this view was unstable; because the support (backup) of the shaft was only a shallow interventricular groove, the tip was easily dislodged. Therefore, another endoscopic control is required to observe the whole heart.

When we gently advanced the endoscope in the I-shape configuration under a fluoroscopic guide (Figure 6, *A, F*), the tip was trapped at the position along the roof (cranial end, Figure 6, *B*) of the pericardial space, between the right ventricular outflow tract and the left atrial appendage. At this position, if we rotated the shaft clockwise and advanced the endoscope with maximally bending the tip

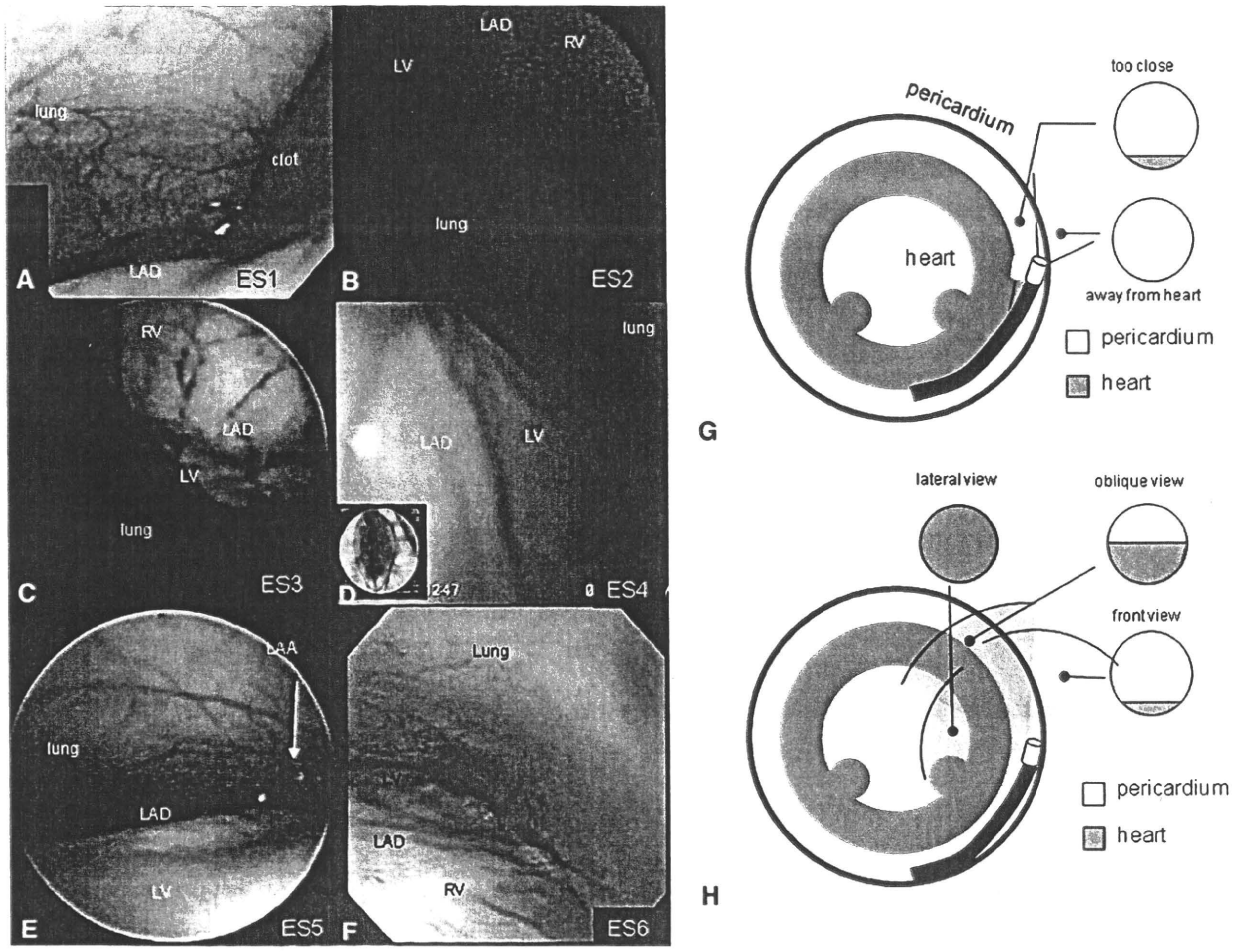

FIGURE 4. A–F, Representative images of left anterior descending artery observed by each endoscope (denoted right bottom, number corresponding to it in Figure 1). It is difficult to front-view the endoscope with a narrow visual angle (A, B). Images of the endoscope without mounting the CCD on the tip (C, E) are fuzzy. Images of the endoscope with the CCD on the tip (D, F) are vivid. G, H, Schematic diagram of spatial configuration of endoscope in the pericardial space and its visual field. G, If the head of the front-view endoscope is directed to the heart surface, the objective lens gets too close to the heart surface. On the other hand, if the endoscope is tipped away from the heart surface, the visual field of the endoscope also tips away from the heart. H, The relation between the visual field and the direction of the objective lens. *LAD*, Left anterior descending artery; *LV*, left ventricle; *ES*, endoscope; *RV*, right ventricle.

(Figure 6, *C*), the tip of the endoscope could be advanced into the right side of the pericardial space. The middle shaft was turned around at the caudal roof of the pericardium, resulting in a so-called inverted U-shape right-side configuration (Figure 6, *D, E, G, H*), allowing the heart to be observed as in a downward-viewing manner (base to apex direction). On the other hand, if we rotated the shaft counterclockwise and advanced the endoscope, the tip of the endoscope could go through the left side of the heart, and a so-called inverted U-shape left-side configuration could be achieved. By use of the inverted U-shape configurations, we could observe every portion of the epicardium (Figure 6, *H*; Video 1).

To effectively control pericardial endoscopy, it is important to take into account the position of backup of the shaft and fulcrum at the point of bending. First, the shaft was fixed at the puncture point of the pericardium. In the I-shape configuration, the shaft was moderately backed up by the anterior interventricular groove, the rotation of the shaft did not help steering devices, and the fulcrum point of bending was only the epicardium. Therefore, it was difficult to keep a distance between the objective lens and the epicardial surface (Figure 4, *G*), resulting in loss of focus and significant halation (Figure 5, *X*). However, when the tip was advanced and bent, the visual field was directed toward the pericardium and kept a distance from the epicardial surface (Figure 4, *G*). Finally, in the inverted U-shape configuration, the middle of the shaft was strongly backed up by the whole pericardium and we could steer the devices by rotating the shaft. This configuration enabled us to keep an appropriate distance from the epicardial surface (Figure 4, *H*; Video 2).

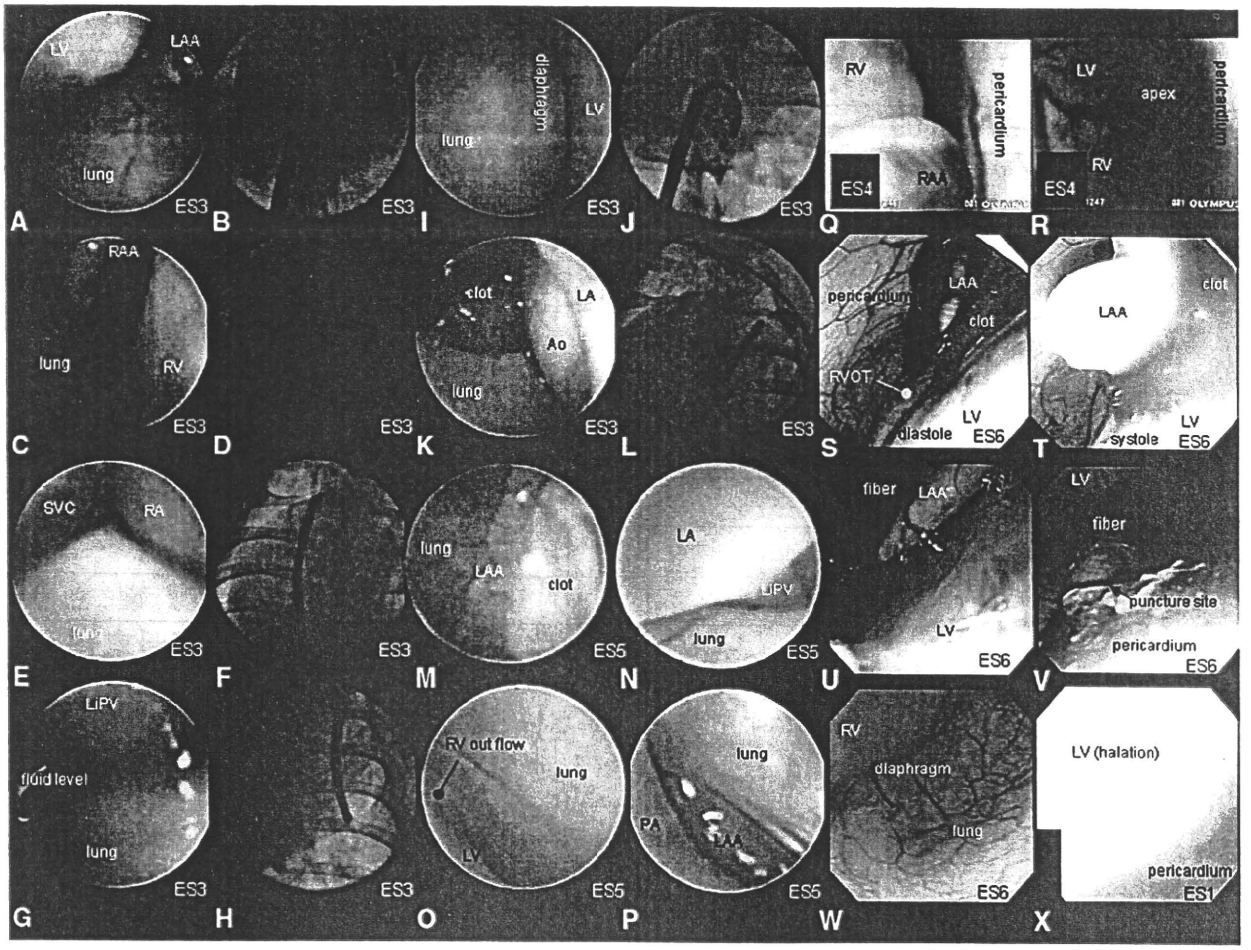

FIGURE 5. Representative images obtained by endoscopy and fluoroscopy. Endoscopic images (A, C, E, G, I, K) obtained by ES3 and corresponding fluoroscopic images (B, D, F, H, J, L, respectively). A, Left atrial appendage and lateral wall of left ventricle. C, Right atrial appendage and lateral wall of right ventricle. E, Superior vena cava and right atrium. G, Left inferior pulmonary vein. I, Pericardium at the diaphragm looks pale compared with pericardium at the lungs. K, Left ventricular outflow tracts. Aortic root and left atrium can be observed. M–P, Endoscopic images obtained by ES5. Left atrial appendage (M, P), left inferior pulmonary vein (N), and pulmonary artery outflow tract (O, P). Q, R, Endoscopic images obtained by ES4. Right atrial appendage (Q), right ventricle (Q, R), and ventricular apex (*apex*, R). S–W, Endoscopic images obtained by ES6. S, T, Sequential image showing dynamic motion of left atrial appendage. U, Left atrial appendage and body of fiber itself. V, Pericardial puncture site and the body of fiber itself. W, Pericardium at the diaphragm. The quality of the images obtained by ES6 is superior to that obtained by ES3. X, Image obtained by ES1. By using the front-view ES with a narrow visual angle, it is difficult to observe the heart surface without significant halation. *Ao*, Aortic; *ES*, endoscopy; *LA*, left atrium; *LAA*, left atrial appendage; *LiPV*, left inferior pulmonary vein; *LV*, left ventricle; *PA*, pulmonary artery; *RA*, right atrium; *RAA*, right atrial appendage; *RV*, right ventricle; *S*, diastole; *SVC*, superior vena cava; *T*, systole.

Feasibility of Minor Surgery

We tested the feasibility of endoscope-guided small operations in the pericardial space. To simulate transplantation of stem cells into the myocardium from the epicardium, we injected Indian ink into the epicardium via endoscope. A 1-mL syringe with 0.2 mL of Indian ink was connected to a 22G needle for endoscopy (NA-201SX-4022; Olympus, Tokyo, Japan). The needle tip was insulated by external Teflon tubing to avoid injury to the coronary vessels. The needle was attached to the surface of the left ventricular free wall via a utility port (Figure 7, *A*). After positioning of the tip, the internal needle was protruded into the myocardium, and then Indian ink was injected without severe hemorrhage (Figure 7, *B*). By protruding the external tube, the objective lens and surface of the heart were stabilized to significantly reduce strong motion artifacts, and adequate working distance was achieved (Figure 7, *C*).

Rigid laparoscopic forceps are essential for endoscope-guided surgery; however, such rigid forceps may compress the heart and deteriorate hemodynamic parameters. Therefore, a flexible endoscope (ES6) and rigid laparoscopic forceps (Figure 7, *E*) were inserted simultaneously to perform

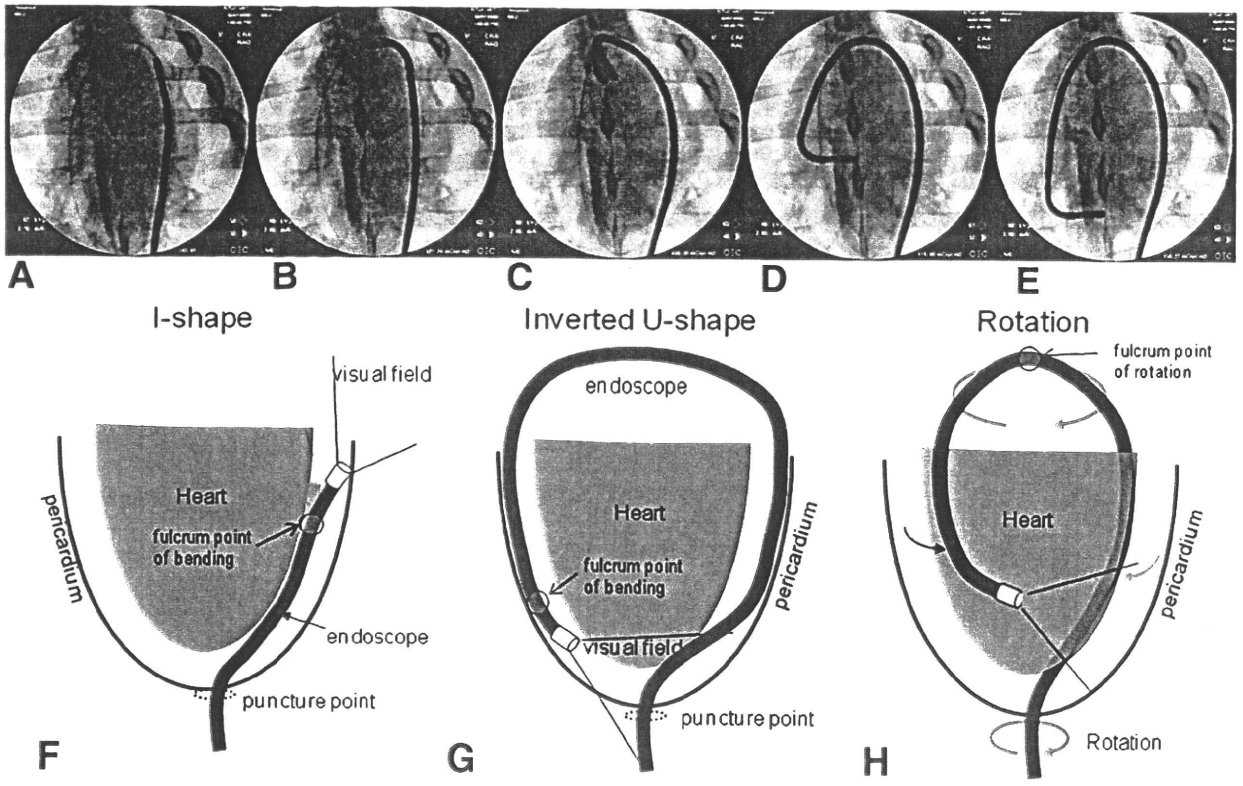

FIGURE 6. A–E, Sequential fluoroscopic images during changing I-shape configuration to inverted U-shape configuration. See details in text. F–H, Schematic diagram of I-shape configuration, inverted U-shape configuration of pericardial endoscope, and how to steer the tip of the endoscope in the pericardial space.

minor surgery (Figure 7, *F–H*). A needle-type pacing electrode (Figure 7, *I*) was transplanted into the left ventricular free wall by use of ES6 (Figure 7, *F–H*). Transplantation was successfully performed without significant hemodynamic change (Figure 7, *J–L*; Video 2).

Complications

Because pericardial endoscopy is the leading minimally invasive technique, the safety of this procedure is our main concern. In the process of puncture by the Seldinger technique, there were no complications, such as hemorrhages, pneumothorax, perforation of left ventricle, or other injuries. During the whole procedure, we could handle the devices in and out numerous times with no changes in blood pressure, pulse oxymetry data, or heart rate (Figure 3) for more than 1 hour. The injection of more than 200 mL of air into the pericardial space suppresses blood pressure by 5 to 10 mm Hg, but blood pressure recovers immediately by removing air from the space via endoscopic utility port.

In terms of chronic phases, pericardial inflammation was evaluated 2 weeks after the operations. There were no macroscopic injuries, coronary stenosis by coronary angiogram, hemorrhages, or adhesion of pericardium (Figure 7, *D*).

DISCUSSION

Selection of Best Endoscope

Because the first priority for pericardial endoscopy is a clear image, an endoscope with a CCD camera on the tip is essential. In popular endoscopes, the objective lens is usually positioned toward an anterior direction (forward-view, ES1, ES2, ES3, ES6). When the endoscope is inserted into the pericardial space, a shaft of the endoscope usually fits along the curve of the epicardial surface, but the objective lens faces toward a tangent direction to the epicardial surface and away from the surface of the heart (Figure 4, *G*). It is reasonable to imagine that positioning the objective lens in a 30- to 60-degree interior oblique direction may be another option (Figure 4, *H*). From an optomechanical point of view, it is difficult to position the lens and CCD complex on the thin tip of endoscopes, although a lens with a 90-degree direction (lateral-view, ES4) can be achieved. Also, so-called fish-eye lenses or wider visual angle lenses (ES3, ES4, ES6) enable observation of the heart surface, even if the distance between the heart and the device is not sufficient.

A diameter less than 6.9 mm with a soft shaft is acceptable, and utility port is necessary for controlling air and devices. Among the ready-made endoscopes, the ES6 showed

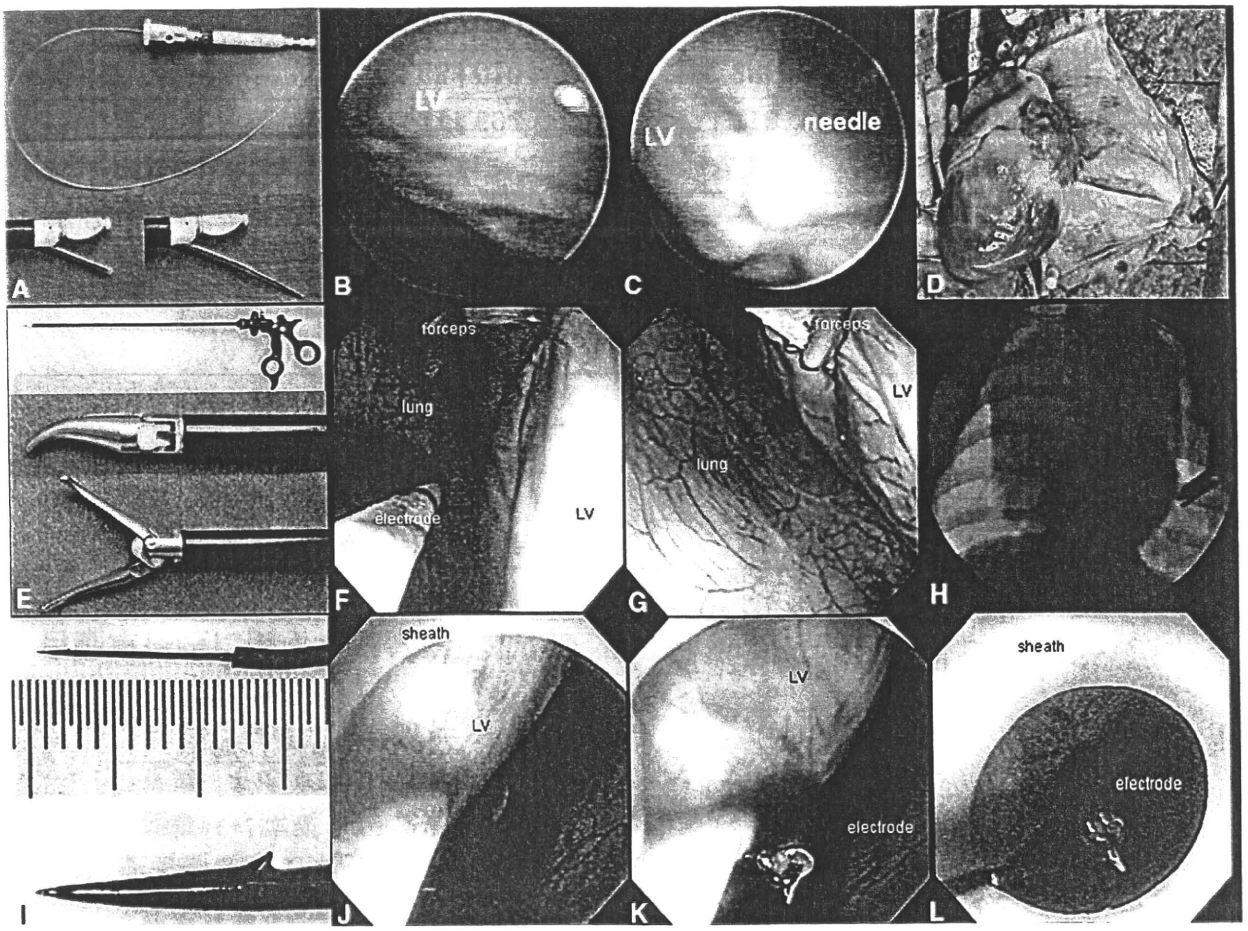

FIGURE 7. A–C, Indian ink was injected into the left ventricular epicardium with a needle. B, Immediately after injection of Indian ink, there was no active bleeding. D, Two weeks after the pericardial endoscopy, there was no coronary injury and no marked adhesion of pericardium. E, Laparoscopic forceps used. *F, G,* Endoscopic (ES6) images during implantation of pacing lead (I) in the left ventricular muscle by using laparoscopic forceps and fluoroscopic images during procedure (H). Implanted pacemaker lead immediately after the implantation (J–L). *LV,* Left ventricle.

the best performance. The ES4 also showed good performance, but there is no utility port for intervention.

Selection of Best Sheath

A certain length of the sheath should be positioned in the pericardial space to obtain back-up support for intervention. By advancing the sheaths, the direction of the sheath is usually perpendicular to the heart surface. A solid sheath causes significant compression of the heart surface and deterioration of hemodynamic parameters. Thus, a floppy sheath is suitable for pericardial endoscopy. Furthermore, to maintain the amount of air within the pericardial space, a check valve at the top of the sheath is essential. Taking this into account, we selected SH4 as the best sheath for pericardial endoscopy.

Stabilization of Motion Artifacts

Stabilization of strong motion artifacts is important. Keeping a distance from the heart surface by use of the inverted U-shape configuration can help stabilize the visual field. Gentle compression of the heart by a rigid manipulator, such as sheaths and laparoscopic forceps, can also stabilize the heartbeat.

Optimization of the Tools

Although we demonstrated the feasibility of the pericardial endoscope by ready-made endoscopes, optimization of the tools should be required. The ES6 is almost acceptable as a pericardial endoscope if we have well-designed forceps for interventions through the utility port. On the other hand, further optimization of the manipulator should be done for pericardial interventions, such as an optimized tool for a cell-delivery system, epicardial pacemaker implantation, and curving of the tip to fit along the heart curvature. The design for the sheath should also be optimized. The optimal material, stiffness, and curve of the sheath remain to be elucidated.

Limitations

Before application for human use, the pericardial endoscopic system should be optimized, and further experiments should be done in other conditions. For example, we did not try the system on an animal with heart failure; therefore, the feasibility of the procedure in the patient with severe heart failure is still undetermined.

We performed the experiment under general anesthesia with respirator support, but for humans this procedure could be performed with local anesthesia. However, in patients with congenital pericardial defect, of which there is a prevalence of 0.0001%[19] to 0.044%,[20] infusion of the gas may cause pneumothorax, so respirator support should be required in such cases.

During this procedure, coincidental occurrence of ventricular fibrillation should be carefully monitored. If this occurs, immediate suction of the gas should be required to perform successful external defibrillation.

It was difficult to observe the posterior surface of the heart because of the limited space between the posterior wall of left atrium and the spine. If the target is the posterior portion of the heart, a lateral position of the patient may gain space and avoid puddling at the focus area. Further experiments should be done for safer procedures.

Clinical Applications

The future of this new technique relies on optimizing its use in humans. Previous studies have demonstrated the effective use of the pericardial approach in the human body, and the device itself is already well known and used clinically. Therefore, there are no obstacles to human application. This method enables us to reach epicardial areas and deep into the myocardium to focus on ablation and implantable cardioverter/defibrillator lead placement in a minimally invasive way. In the present study, we infused air into the pericardial space. However, there is less chance of causing air embolism and significant mediastinal emphysema with carbon dioxide compared with air. For clinical application, infusion of carbon dioxide gas is considered to be safer in this system.

Moreover, in cardiac stem cell therapy, there is no standard method of stem cell transplantation. Transplantation via coronary vessels may not deliver the cells to the appropriate location in the heart tissue, may occlude coronary vessels, and may generate additional myocardial infarctions.[7] Direct injection into the myocardium from an endocardial site via a needle devised on the tip of a catheter using an electroanatomic mapping system (NOGA System, Biosense Webster, Markham, ON, Canada)[6] is similar to the common catheter ablation procedure. Although the catheter procedure is safe and can be performed repeatedly, the injected cells may backflush into the left ventricular cavity via needle trajectory and disseminate into the systemic circulation, causing systemic microembolizations. From this point of view, injection of the cells from the epicardial surface is secure. However, open chest surgery is required to avoid coronary vessels. Pericardial endoscopy-guided cellular transplantation from the epicardial surface can be a major method for stem cell transplantation.

CONCLUSIONS

Our experiment has established a new and simple method for obtaining a clear view of the pericardial space with the use of pericardial endoscopy. The percutaneous subxyphoid approach using the Seldinger technique was useful and safe. An x-ray fluoroscopic guide was necessary to steer the endoscope in the pericardial space. We have shown short- and long-term safety with regard to hemodynamic changes, infections, and adhesion of pericardium. Pericardial endoscopy can introduce a new era of technology for cardiac surgeons and cardiac interventionists.

The authors thank Olympus Corporation for technical advice and Satoshi Ogawa MD, PhD, and Toshiaki Satoh, MD, PhD, for medical advice.

References

1. Gruntzig AR, Senning A, Siegenthaler WE. Nonoperative dilatation of coronary-artery stenosis: percutaneous transluminal coronary angioplasty. *N Engl J Med*. 1979;301:61-8.
2. Gallagher JJ, Svenson RH, Kasell JH, German LD, Bardy GH, Broughton A, et al. Catheter technique for closed-chest ablation of the atrioventricular conduction system. *N Engl J Med*. 1982;306:194-200.
3. Scheinman MM, Morady F, Hess DS, Gonzalez R. Catheter-induced ablation of the atrioventricular junction to control refractory supraventricular arrhythmias. *JAMA*. 1982;248:851-5.
4. Abraham WT, Fisher WG, Smith AL, Delurgio DB, Leon AR, Loh E, et al. Cardiac resynchronization in chronic heart failure. *N Engl J Med*. 2002;346:1845-53.
5. Cribier A, Eltchaninoff H, Bash A, Borenstein N, Tron C, Bauer F, et al. Percutaneous transcatheter implantation of an aortic valve prosthesis for calcific aortic stenosis: first human case description. *Circulation*. 2002;106:3006-8.
6. Perin EC, Dohmann HF, Borojevic R, Silva SA, Sousa AL, Mesquita CT, et al. Transendocardial, autologous bone marrow cell transplantation for severe, chronic ischemic heart failure. *Circulation*. 2003;107:2294-302.
7. Vulliet PR, Greeley M, Halloran SM, MacDonald KA, Kittleson MD. Intra-coronary arterial injection of mesenchymal stromal cells and microinfarction in dogs. *Lancet*. 2004;363:783-4.
8. Breitbach M, Bostani T, Roell W, Xia Y, Dewald O, Nygren JM, et al. Potential risks of bone marrow cell transplantation into infarcted hearts. *Blood*. 2007;110:1362-9.
9. Kikuchi K, McDonald AD, Sasano T, Donahue JK. Targeted modification of atrial electrophysiology by homogeneous transmural atrial gene transfer. *Circulation*. 2005;111:264-70.
10. Ota T, Degani A, Zubiate B, Wolf A, Choset H, Schwartzman D, et al. Epicardial atrial ablation using a novel articulated robotic medical probe via a percutaneous subxiphoid approach. *Innovations Phila Pa*. 2006;1:335-40.
11. Soejima K, Couper G, Cooper JM, Sapp JL, Epstein LM, Stevenson WG. Subxiphoid surgical approach for epicardial catheter-based mapping and ablation in patients with prior cardiac surgery or difficult pericardial access. *Circulation*. 2004;110:1197-201.

12. Soejima K, Stevenson WG, Sapp JL, Selwyn AP, Couper G, Epstein LM. Endocardial and epicardial radiofrequency ablation of ventricular tachycardia associated with dilated cardiomyopathy: the importance of low-voltage scars. *J Am Coll Cardiol*. 2004;43:1834-42.
13. Maisch B, Bethge C, Drude L, Hufnagel G, Herzum M, Schonian U. Pericardioscopy and epicardial biopsy—new diagnostic tools in pericardial and perimyocardial disease. *Eur Heart J*. 1994;15(Suppl C):68-73.
14. Seferovic PM, Ristic AD, Maksimovic R, Tatic V, Ostojic M, Kanjuh V. Diagnostic value of pericardial biopsy: improvement with extensive sampling enabled by pericardioscopy. *Circulation*. 2003;107:978-83.
15. Nazarian S, Kantsevoy SV, Zviman MM, Matsen FA 3rd, Calkins H, Berger RD, et al. Feasibility of endoscopic guidance for nonsurgical transthoracic atrial and ventricular epicardial ablation. *Heart Rhythm*. 2008;5:1115-9.
16. Gerosa G, Bianco R, Buja G, di Marco F. Totally endoscopic robotic-guided pulmonary veins ablation: an alternative method for the treatment of atrial fibrillation. *Eur J Cardiothorac Surg*. 2004;26:450-2.
17. Zenati MA, Bonanomi G, Chin AK, Schwartzman D. Left heart pacing lead implantation using subxiphoid videopericardioscopy. *J Cardiovasc Electrophysiol*. 2003;14:949-53.
18. Spodick DH. The technique of pericardiocentesis. When to perform it and how to minimize complications. *J Crit Illn*. 1995;10:807-12.
19. Southworth H, Stevenson CS. Congenital defects of the pericardium. *Arch Intern Med*. 1938;223-40.
20. Van Son JA, Danielson GK, Schaff HV, Mullany CJ, Julsrud PR, Breen JF. Congenital partial and complete absence of the pericardium. *Mayo Clin Proc*. 1993; 68:743-7.

000 Safety and efficacy of pericardial endoscopy by percutaneous subxyphoid approach in swine heart in vivo

Takehiro Kimura, MD, Shunichiro Miyoshi, MD, PhD, Seiji Takatsuki, MD, PhD, Kojiro Tanimoto, MD, PhD, Kotaro Fukumoto, MD, PhD, Kyoko Soejima, MD, PhD, and Keiichi Fukuda, MD, PhD, Tokyo and Kawasaki, Japan

As the pioneer of the novel minimally invasive surgery, we have demonstrated the safety and feasibility of pericardial endoscopy. We have established the techniques to obtain clear images by selecting appropriate devices in swine and succeeded in performing interventions such as cell transplantation and pacemaker lead implantation with no complications.

Stem Cell Research (2011) 6, 83–89

available at www.sciencedirect.com

ScienceDirect

www.elsevier.com/locate/scr

SHORT REPORT

Simple autogeneic feeder cell preparation for pluripotent stem cells

Weizhen Li [a,1], Hiromi Yamashita [a,1], Fumiyuki Hattori [a,b,*], Hao Chen [a], Shugo Tohyama [a], Yusuke Satoh [a,c], Erika Sasaki [d], Shinsuke Yuasa [a], Shinji Makino [a], Motoaki Sano [a], Keiichi Fukuda [a,*]

[a] *Division of Cardiology, Department of Medicine, Keio University School of Medicine, 35 Shinanomachi, Shinjuku-ku, Tokyo 160-8582, Japan*
[b] *Asubio Pharma Co., Ltd. 6-4-3, Minatojimaminami-cho, Chuo-ku, Kobe-city, Hyogo 650-0047, Japan*
[c] *Division of Basic Biological Sciences, Keio University Faculty of Pharmacy, 1-5-30 Shibakoen, Minato-ku, Tokyo 105-8512, Japan*
[d] *Department of Applied Developmental Biology, Central Institute for Experimental Animals, 1430 Nogawa, Miyamae-ku, Kawasaki, Kanagawa 216-0001, Japan*

Received 17 July 2010; received in revised form 21 September 2010; accepted 21 September 2010

Abstract Mouse embryonic fibroblasts (MEFs) are the most commonly used feeder cells for pluripotent stem cells. However, autogeneic feeder (AF) cells have several advantages such as no xenogeneic risks and reduced costs. In this report, we demonstrate that common marmoset embryonic stem (cmES) cells can be maintained on common marmoset AF (cmAF) cells. These cmES cells were maintained on cmAF cells for 6 months, retaining their morphology, normal karyotype, and expression patterns for the pluripotent markers Oct-3/4, Nanog, SSEA-3, SSEA-4, TRA-1-60, and TRA-1-81, as well as their ability to differentiate into cardiac and neural cells. Antibody array analysis revealed equivalent protein expression profiles between cmES cells maintained on cmAF cells and MEFs. In addition, similarly prepared human embryonic stem (hES) and induced pluripotent stem (hiPS) cell-derived AF cells supported the growth of and maintained the morphology and pluripotent marker expressions of hES and hiPS cells, respectively. DNA microarray analysis revealed that these hES and hiPS cells had mRNA expression profiles similar to those of hES and hiPS cells maintained on MEFs, respectively. Taken together, these findings imply that AF cells can replace MEFs in the routine maintenance of primate pluripotent stem cells.

Introduction

Since human embryonic stem (hES) cells were first established by Thomson et al. in 1998, promising results have been obtained with these cells (Thomson et al., 1998). However, owing to ethical problems and concerns about clinical safety, hES cells have not yet been used in clinical studies. Nonhuman primates and their ES and induced pluripotent stem (iPS) cells are expected to be effective preclinical models given their close genetic relationships to humans, as compared with

* Corresponding authors. F. Hattori is to be contacted at Division of Cardiology, Department of Medicine, Keio University School of Medicine, 35 Shinanomachi, Shinjuku-ku, Tokyo 160-8582, Japan. Fax: +81 3 5363 3875. K. Fukuda, fax: +81 3 5363 3875.
E-mail addresses: hattori.fumiyuki.ef@asubio.co.jp (F. Hattori), kfukuda@sc.itc.keio.ac.jp (K. Fukuda).
[1] Weizhen Li and Hiromi Yamashita equally contributed to this study.

1873-5061/$ – see front matter © 2010 Elsevier B.V. All rights reserved.
doi:10.1016/j.scr.2010.09.003

rodents (Hearn, 2001; Nakatsuji and Suemori, 2002). Sasaki and co-workers recently established common marmoset ES (cmES) and iPS cell lines, and green fluorescent protein (GFP)-transgenic marmosets (Sasaki et al., 2005; Sasaki et al., 2009; Tomioka et al., 2010), and described the efficient differentiation of neural cells from cmES cells (Sasaki et al., 2005). Chen et al. also reported successful differentiation of cardiomyocytes from cmES cells and described their characterization (Chen et al., 2008).

Recently, iPS cells have been established in rodents (Takahashi and Yamanaka, 2006), nonhuman primates (Tomioka et al., 2010; Wu et al., 2010; Liu et al., 2008), and humans (Takahashi et al., 2007). Clinical applications for these cells are also eagerly awaited, since iPS cells with a genetic background identical to that of the patient can be generated with less ethical concerns. Even though several improvements have been made to combat initial problems, clinical application of human iPS (hiPS) cells is still controversial due to a number of safety concerns.

Common technical constraints for the therapeutic application of hES and hiPS cells also remain. One such limitation is avoiding the use of xenogeneic materials, since there is a risk of cross-transfer of potential pathogens and unexpected genes. To date, various xenogeneic factor-free culture methods have been developed to replace the MEFs used for culturing hES cells, such as immortalized MEFs (Choo et al., 2006), Matrigel (Xu et al., 2001; Akopian et al., 2010), mixed extracellular matrix (Amit and Itskovitz-Eldor, 2006), human-derived primary (Cheng et al., 2003; Lee et al., 2005) and immortalized feeder cells (Unger et al., 2009), suspension culture systems (Steiner et al., 2010; Singh et al., 2010; Olmer et al., 2010; Amit et al., 2010), and autogeneic feeder (AF) cells (Amit and Itskovitz-Eldor, 2006; Choo et al., 2008; Stojkovic et al., 2005; Wang et al., 2005), as well as several xenogeneic factor-free media (Akopian et al., 2010) which can be combined with xeno-free feeders and feeder-free methods. Nevertheless as shown in the report from the International Stem Cell Initiative, most xenogeneic factor-free culture systems based on feeder-free conditions are biased toward hES cell lines (Akopian et al., 2010), suggesting that the MEF feeder system remains the standard because it ensures stable and reliable maintenance for every pluripotent stem cell line. Also in our hands, the MEF feeder system is still the most reliable and general method for maintaining cmES and hES cells, and hiPS cells. Therefore, it is necessary to develop further options for alternative human feeder cells.

AF systems for hES cells have been reported by two groups; the first group derived AF cells via embryoid body (EB) formation (Stojkovic et al., 2005), while the second group generated a stable cell line from differentiated hES cells (Choo et al., 2008). In the present report, we describe a novel method for the preparation of AF cells derived from spontaneously differentiated cells for use in the routine maintenance of pluripotent stem cells. In addition, we report a common method for the preparation of AF cells for different nonhuman primate and human pluripotent stem cells.

Results

Under our routine experimental conditions, cmES, hES, and hiPS cells stably self-renew on MEFs. However a small fraction of each colony contains spontaneously differentiated cells that have sprouted from the edges of the colonies. During routine passaging, we found that the weak trypsin and collagenase treatment detached preferentially the undifferentiated cells of the colonies, leaving the differentiated cells attached to the plate (Fig. 1a). Since the detached cells had features typical of fibroblasts, we expected that they could be used as AF cells. Previously, these cells would have been discarded, so we term our AF preparation the "cell recycling system." The principle underlying this phenomenon is shown in Fig. 1b.

We cultured the residual cells for 2–4 weeks until they reached subconfluence. The cultivation period to the first passage varied depending on the initial concentration of differentiated cells. The period of time between the passages was approximately 3–5 days. Between the first and third passages, we estimated that the cells had a doubling time of about 20 h. To investigate the relationship between passage number and ability to maintain the undifferentiated state of the cmES cells, we seeded cmES cell clumps onto mitomycin C-treated cmAF cells of various passage numbers, and observed the morphology of the cells under the microscope (Fig. 1c). We found that the cmAF cells that underwent up to three passages maintained the cmES cells without any obvious morphologic alteration of the cmES cells (Fig. 1c). In contrast, when we used cmAF cells after the fourth passage, we found a significant decrease in their maintenance capability. Therefore, we used cmAF cells at the third passage for routine culturing of cmES cells. cmAF cells that were freshly treated with mitomycin C could maintain cmES cells for 1 week; thereafter, they showed decreased viability and maintenance ability. To investigate whether residual MEFs were diluted during cmAF expansion, we performed immunohistochemical analysis for human nuclear antigen (Chen et al., 2008) on cultures of cmAF cells. We found no human nuclear antigen-negative cells (residual MEFs) by fluorescent microscopy (Fig. 1d), which meant that the MEFs had been eliminated during the three passages. The mitomycin C-treated and untreated cmAF cells were successfully stored in the long-term using slow-freezing methods. The viability of the recovered cmAF cells was typically 80 to 90%.

We prepared consecutive batches of cmAF cells from cmES cells that had been cultured on cmAF cells, and maintained the cmES cells in this system for more than 6 months. The cmES cells cultured on cmAF cells for 6 months expressed Oct-3/4, Nanog, SSEA-3, SSEA-4, TRA-1-60, and TRA-1-81 (Fig. 2a). We also confirmed that the cmES cells possessed alkaline phosphatase activity, which is a typical feature of pluripotent stem cells (Fig. 2a). Cytogenetic analysis of the cmES cells that were long-term-cultured on cmAF cells revealed that they retained the normal karyotype of 46XX (Fig. 2b).

To investigate the differentiation ability of the cmES cells cultured on cmAF cells, we induced cardiogenic and neurogenic differentiation. The cmES cells differentiated into cardiomyocytes via embryoid body formation (Fig. 3a). We partially dispersed the EBs and attached them to fibronectin-coated dishes. Immunohistochemical analysis revealed that the EBs expressed Nkx2.5 and sarcomeric α-actinin, indicating that they were cardiomyocytes (Fig. 3b, left panel). We induced neurogenic differentiation by serum withdrawal and retinoic acid stimulation. Thus, we observed sprouting filamentous cells from the attached core of the EBs (Fig. 3b, right panel). We demonstrated immunofluorescence staining for βIII tubulin,

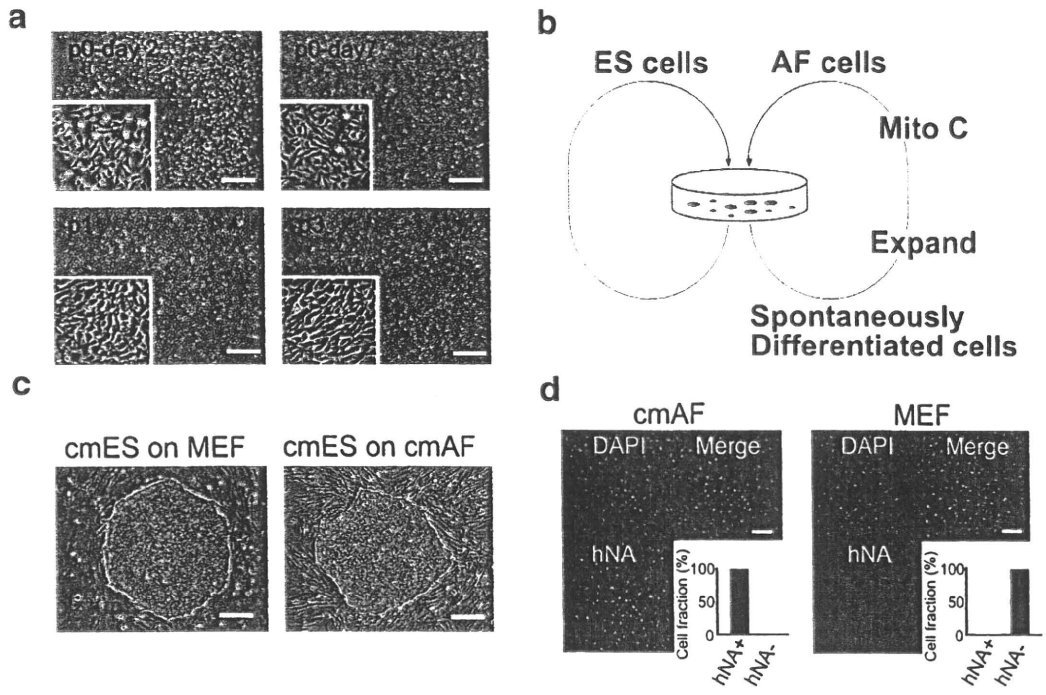

Figure 1 Preparation and application of cmAF cells to cmES cell culturing. (a) Spontaneously differentiated cells that remain on the culture dish are expanded. (b) Schematic representation of the preparation of cmAF cells and the culturing of cmES cells. (c) Morphology of cmES cells cultured on either MEFs (left) or cmAF cells (right). (d) Absence of MEF contamination in the cmAF cells (p3). The right panel shows MEFs used as a negative control in the immunohistochemical detection of human nuclear antigen (hNA). Scale bars: (a and c) 500 μm; (d) 200 μm.

which is a marker for mature neurons, and confirmed that some of the cells expressed βIII tubulin.

Furthermore, to demonstrate the similarity of cmAF cells and MEFs, we analyzed the protein expression profiles of cmES cells cultured on cmAF cells and MEFs, taking advantage of antibody (protein) arrays that are applicable to a broad range of species from rodents to humans. We used the Panorama antibody microarray XP725 kit, which consists of 725 antibodies that have been validated by the manufacturer for studies of mouse and human samples. These antibodies represent families of proteins known to be involved in a variety of important biological pathways, including cell signaling, matrix processing, cell growth, and apoptosis. We analyzed Cy3 labeling of the total protein extracts from cmES cells cultured on cmAF cells or MEFs. Each Cy3-labeled protein was bound to an individual antibody-arrayed glass slide. The fluorescent signals were evaluated using a scanner (Fig. 3c, left). Few proteins had greater than twofold expression changes between cmES cells cultured on cmAF cells and MEFs, indicating that cmES cells cultured on cmAF cells and MEFs have similar protein expression profiles (Fig. 3c, right). We also compared cmES cells cultured on cmAF cells with purified common marmoset ES cell-derived cardiomyocytes as a control experiment. Several differences in protein expression were observed between the cmES cells and purified cardiomyocytes; these included proteins reported to be expressed in cardiomyocytes, such as histone deacetylase 2 (Lu and Yang, 2009), estrogen receptor, and in pluripotent stem cells, such as mitogen and stress activated kinase (Arthur and Cohen, 2000), C-src tyrosine kinase, and Coffilin (Fig. 3d).

Next, we applied our feeder preparation method to hES and hiPS cells (Fig. 4). The hAF and hiAF cells prepared from hES and hiPS cells were found to maintain hES and hiPS cells for more than 2 months, respectively (Fig. 4a). To investigate whether the MEFs were diluted during the expansion of hiAF cells, we performed immunofluorescent staining for human nuclear antigens with analysis by FACS. Almost all the prepared hiAF cells were positive for human nuclear antigen (Fig. 4b). To further investigate whether the MEFs were diluted during the expansion of hAF cells, we used a stably GFP-expressing hES cell line for hAF cell preparation. We randomly observed five visual fields under the microscope. As a result, no GFP-negative cells (MEFs) were found in the prepared hAF cells (Supplementary Fig. 2). Taken together, these findings show that residual MEFs are eliminated in hiAF cells. Next, we investigated the pluripotency of hiPS cells maintained on hiAF cells by immunofluorescent stainings including microscopic observation (Supplementary Fig. 3) and FACS analysis of SSEA-4, TRA-1-81, Nanog, and Oct-3/4, and confirmed that almost all the hiPS cells expressed the four pluripotent markers (Fig. 4c). We also performed DNA expression array analysis of the hES and hiPS cells that were maintained long-term on hAF and hiAF cells, respectively. Equivalent mRNA expression levels of the pluripotency-related genes including *oct-3/4*, *nanog*, *sox-2*, *lin28*, and *c-myc* were observed. Global gene expression profiles were also quite similar in both cases (Fig. 4d, left). In contrast, two comparative expression profiles between hES and hiPS cells and their differentiating EBs indicated the marked existence of differentially expressed genes (Fig. 4d, right). In addition, a similar magnitude of difference to the results shown in the left panel of Fig. 4d was seen when comparing global gene expression profiles for hES and hiPS cells during different passage numbers (Supplementary Fig. 4). All these results show

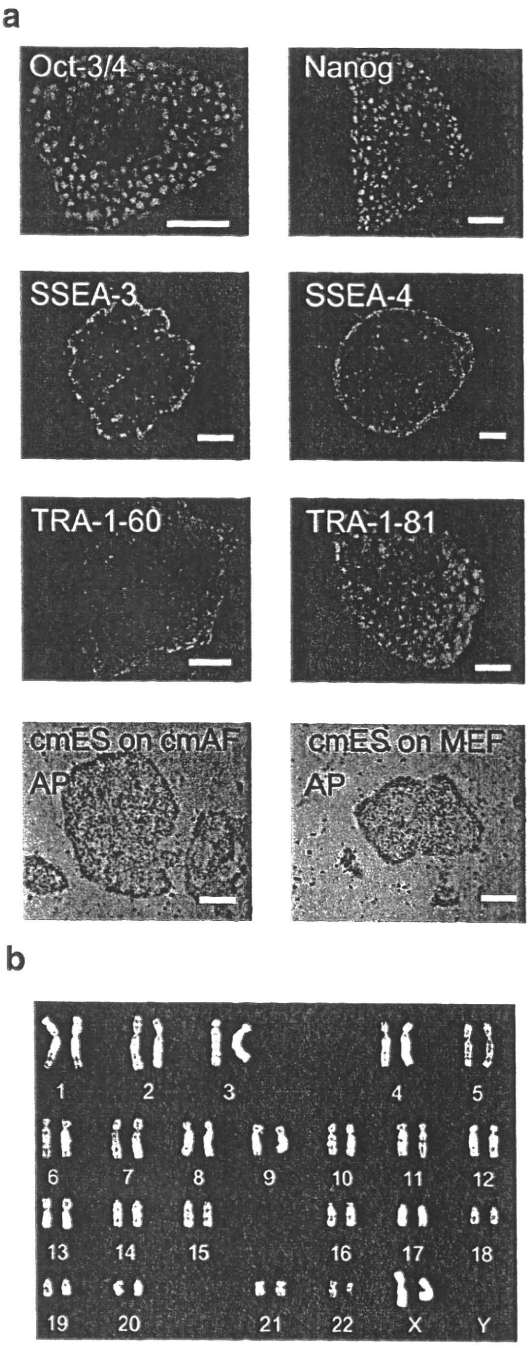

Figure 2 Pluripotent marker expression and cytogenetic analyses of cmES cells cultured on cmAF cells. (a) Immunofluorescence staining for Oct-3/4, Nanog, SSEA-3, SSEA-4, TRA-1-30, and TRA-1-80 of cmES cells cultured on cmAF cells for 6 months. Alkaline phosphatase activities of cmES cells cultured on either cmAF cells (left panel) or MEFs (right panel). (b) Cytogenetic analysis of cmES cells cultured on cmAF cells for 6 months. Scale bar: (a) 300 μm.

that our hAF and hiAF cells can maintain hES cells in an undifferentiated state and in a condition quite similar to that achieved with MEFs.

Discussion

We have demonstrated the preparation of AF cells from three different cell sources using a common method. These AF cells succeeded in effectively maintaining their pluripotent stem cells.

In this study, we used antibody array analyses to characterize cmES cells. Quite similar protein expression profiles were observed between cmES cells cultured on cmAF cells and MEFs. However, in contrast, various differentially expressed proteins were observed in purified cmES cell-derived cardiomyocytes compared to cmES cells. These results validate the usefulness of this system, and indicate a similar efficacy of cmAF cells compared to MEFs for the maintenance of cmES cells. The mRNA expression profiles produced by global gene array analyses comparing hES cells cultured on hAF cells and MEFs and hiPS cells cultured on hiAF cells and MEFs revealed an overall high similarity in profiles; however, they were not perfectly identical. The differential gene expression profiles comparing different passage numbers of the same human pluripotent stem cells maintained with the same feeder cells showed a similar dispersion to those observed between human pluripotent stem cells maintained with MEF and AF cells. These results suggest that some allowable gene expression changes might spontaneously occur during long-term culture in pluripotent stem cells, although the genes related with pluripotency must be maintained.

Using our routine preparation of cmAF cells, approximately 1×10^8 cells can be obtained from a single 10-cm dish and three cell passages. This number of cmAF cells is sufficient to prepare 100 10-cm dishes for cmES cell culturing. In contrast, 1×10^7 MEFs are typically obtained from a single mouse embryo under our experimental conditions. Thus we believe that our AF system has a comparable cell yield to that of the MEF system.

As potential therapies using personalized iPS cells become possible, it may be reasonable to maintain an individual's hiPS cell line using their AF cells, because there would be no concerns of transfer of allogenic antigens or infectious viruses from the feeder cells. Even in the case of mass production of therapeutic cells from banked pluripotent stem cells, techniques have not yet been established for maintaining pluripotent stem cells under xenogeneic factor-free conditions at a reasonable cost.

Conclusions

The present study establishes an effective method for preparing AF cells which is applicable to cmES, hES, and hiPS cells. We believe that the results of the present study pave the way for the reliable and economic production of alternative feeder cells for pluripotent stem cells.

Materials and methods

Maintenance of undifferentiated cmES, hES cells, and hiPS cells

The cmES cells (cell line No. 20; Central Institute of Experimental Animals, Kawasaki, Japan), hES cells (khES-2; Institute for Integrated Cell-Material Sciences, Kyoto University), and hiPS cells (G4; Center for iPS Cell Research and

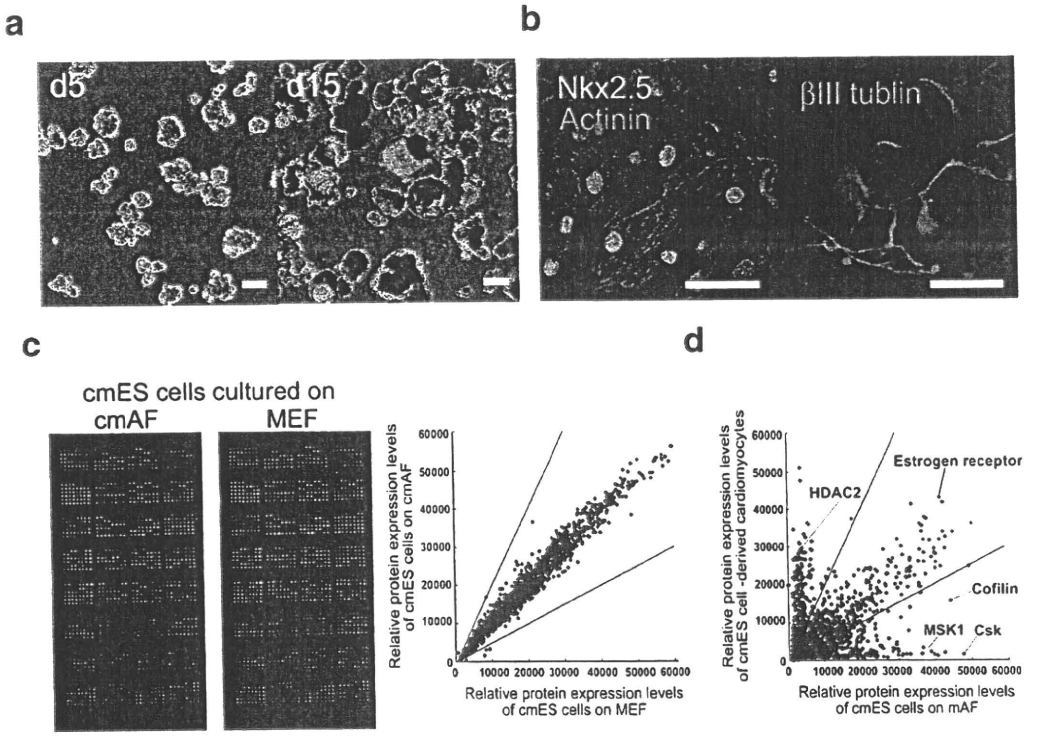

Figure 3 *In vitro* differentiation abilities of the cultured cmES cells and antibody array analysis of cmES cells cultured on either cmAF cells or MEFs. (a) EB formation of cmES cells during long-term culturing on cmAF cells. (b) Cardiomyocytes and neurons differentiate from cmES cells during long-term culturing on cmAF cells. (c) Antibody array analysis was performed on Cy3-labeled total protein extracts from cmES cells cultured on either cmAF cells or MEFs for 50 days. The left panels show the raw images of the Cy3 signals. The scatter plot shows the relative fluorescence levels for the antibodies used to stain cmES cells cultured on cmAF cells (*y*-axis) and MEFs (*x*-axis). (d) Antibody array analysis was performed on protein extracts from cmES cells cultured on cmAF cells and purified cmES cell-derived cardiomyocytes. The scatter plot shows the relative fluorescence levels for the antibodies used to stain purified cmES cell-derived cardiomyocytes (*y*-axis) and cmES cells cultured on cmAF cells (*x*-axis). Twofold differences, representing the threshold in this experiment, are indicated as lines in the plots (c, d). Scale bars: (a) 300 μm; (b) 100 μm.

Application, Institute for Integrated Cell-Material Sciences, Kyoto University) were maintained as described previously (Chen et al., 2008; Hattori et al., 2010). Briefly, cmES cells were maintained on feeder cells in cmES cell medium, which consisted of 80% Knockout Dulbecco's modified Eagle's medium (KO-DMEM; Invitrogen, Carlsbad, CA, USA), 20% Knockout Serum Replacement (KSR; Invitrogen), 0.1 mM nonessential amino acids (Sigma Chemical Company), 2 mM L-glutamine (Sigma, St. Louis, MO), 0.1 mM β-mercaptoethanol (Sigma), and 4 ng/mL basic fibroblast growth factor (Wako Pure Chemical Industries, Osaka, Japan). hES and hiPS cells were similarly maintained, except that Dulbecco's modified Eagle's medium/Nutrient Mixture F-12 Ham's (1/1 ratio, DMEM-F12; Sigma) was used instead of KO-DMEM. The cmES and hES cells were passaged every 5–7 days. Typically, we cultured pluripotent stem cells in 15-cm dishes (Becton–Dickinson, NJ, USA). Using this method, all reagent amounts were suitable for 15-cm dish cultures.

Passage of pluripotent stem cells

All cmES, hES, and hiPS cells were treated with 2 mL of 0.25% trypsin (Becton–Dickinson), 0.1% collagenase type 3 (Worthington Biochemical Corp., NJ, USA), 20% KSR, and 1 mM $CaCl_2$ in phosphate-buffered saline at 37 °C for 5–15 min, which resulted in disruption of the boundaries between the pluripotent stem cells and the feeder cells. Then, 5 mL of DMEM supplemented with 10% fetal bovine serum (FBS; Biowest, FL, USA) was added and the cells were gently pipetted several times, which detached all the pluripotent stem cell colonies and most of the feeder cells from the dish. The cells were separated into three fractions by size, <40 μm, between 40 and 100 μm, and >100 μm, using cell strainers with mesh pore diameters of 40 and 100 μm (Becton–Dickinson). These procedures are illustrated in Supplementary Fig. 1a. This process eliminated feeder cells (Supplementary Fig. 1b). The collected pluripotent stem cell colonies of the correct size (larger than 40 μm and smaller than 100 μm) were seeded onto a new plate with feeder cells.

Preparation of AF cells

A low number of differentiating cells remained on the culture dish after passage (Fig. 1a). These cells were the seeds of the AF cells, and they were propagated in DMEM (Wako) supplemented with 10% FBS. Typically, propagation to near confluence took 10–15 days for cmAF cells and 20–30 days for human AF (hAF) and iAF (hiAF) cells. For passaging, the cells were detached and dispersed by treatment with 0.25% trypsin-EDTA solution (TE; Invitrogen) at 37 °C for 10 min. A cell

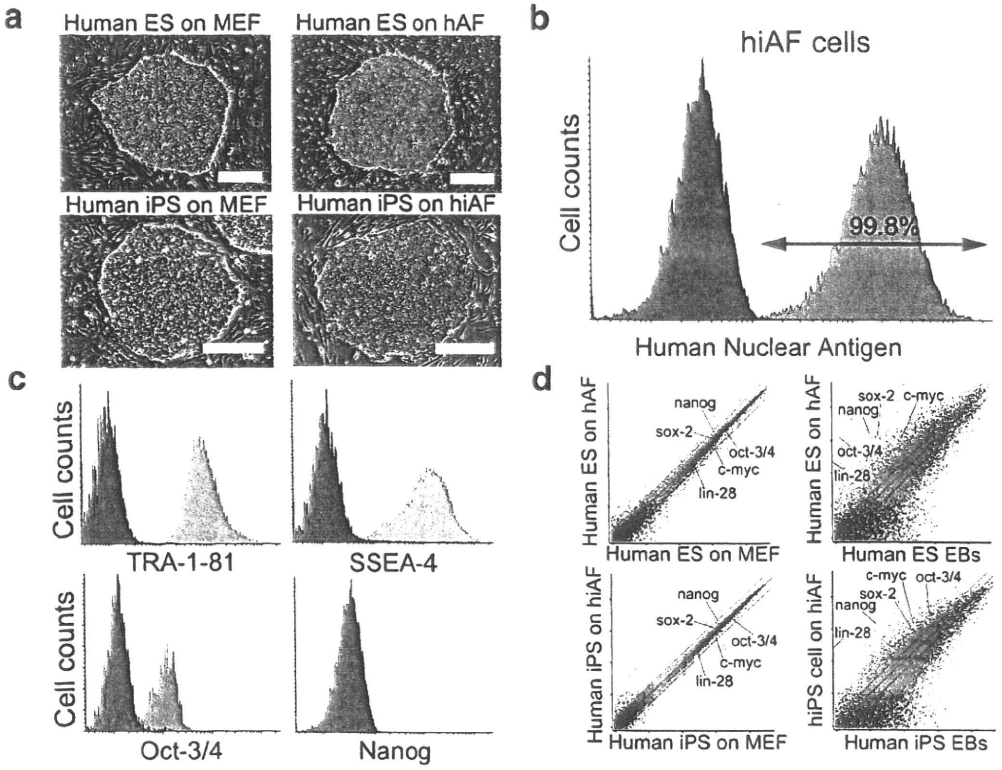

Figure 4 Application of hAF and hiAF cells to the cultivation of hES and hiPS cells, and DNA microarray analysis. (a) Morphology of hES (upper panels) and hiPS (lower panels) cells cultured on either MEFs (left panels) or hAF and hiAF cells (right panels). (b) Human nuclear antigen was immunofluorescently detected and analyzed by FACS (red histogram) in the hiAF cells. The negative control (second antibody only) is shown as the blue histogram. (c) Human iPS cells which were maintained long term by hiAF cells were passaged, as described under Materials and methods, enzymatically dispersed, immunofluorescently stained for TRA-1-81, SSEA-4, Oct-3/4, and Nanog, and then analyzed by FACS. The negative control (second antibody only) is shown as the blue histogram. (d) DNA microarray analysis of mRNA extracted from hES (upper left panel) and hiPS (lower left panel) cells that were cultured on either hAF and hiAF cells (y-axis) or MEFs (x-axis) for 32 or 35 days, respectively. Similarly, comparisons between hES cells grown on hAF cells (upper) or hiPS cells grown on hiAF cells (lower) and their EBs are shown in the right panels. The scatter plot shows the relative expression level (threshold:10) for each gene. Twofold differences are indicated as lines in the plot. Scale bars: (a) 300 μm.

strainer with mesh pore diameter of 40 μm (Becton-Dickinson) was used to eliminate the residual large cell clumps (diameter >40 μm). The purified AF cells were plated onto new 0.1% gelatin-coated dishes that contained DMEM supplemented with 10% FBS. For all the cmES, hES, and hiPS cells, confluence was achieved in 3–5 days, and these cells were subsequently passaged to the next generation using a 5-times dilution. The second or third generation of AF cells were treated with 10 μg/mL of mitomycin C at 37 °C for 3 h, and cryopreserved at -150 °C in Cellbanker solution (Mitsubishi Chemical, Tokyo, Japan). The cmAF, hAF, or hiAF cells recovered from the cryostocks were seeded onto 0.1% gelatin-coated dishes at a concentration of 2×10^6 cells per 15-cm dish.

Supplementary materials related to this article can be found online at doi:10.1016/j.scr.2010.09.003.

Acknowledgments

This study was supported in part by research grants from the Special Coordination Funds for Promoting Science and Technology in the Japanese Ministry of Education, Culture, Sports, Science, and Technology and from the Japan-China Medical Association. This work was also in part surported by KAKENHI and New Energy and Industrial Technology Development Organization (NEDO).

References

Akopian, V., Andrews, P.W., Beil, S., Benvenisty, N., Brehm, J., Christie, M., Ford, A., Fox, V., Gokhale, P.J., Healy, L., Holm, F., Hovatta, O., Knowles, B.B., Ludwig, T.E., McKay, R.D., Miyazaki, T., Nakatsuji, N., Oh, S.K., Pera, M.F., Rossant, J., Stacey, G.N., Suemori, H., 2010. Comparison of defined culture systems for feeder cell free propagation of human embryonic stem cells. In Vitro Cell. Dev. Biol. Anim. 46, 247–258.

Amit, M., Itskovitz-Eldor, J., 2006. Feeder-free culture of human embryonic stem cells. Methods Enzymol. 420, 37–49.

Amit, M., Chebath, J., Margulets, V., Laevsky, I., Miropolsky, Y., Shariki, K., Peri, M., Blais, I., Slutsky, G., Revel, M., Itskovitz-Eldor, J., 2010. Suspension culture of undifferentiated human embryonic and induced pluripotent stem cells. Stem Cell Rev. 6, 248–259.

Arthur, J.S., Cohen, P., 2000. MSK1 is required for CREB phosphorylation in response to mitogens in mouse embryonic stem cells. FEBS Lett. 482, 44–48.

Chen, H., Hattori, F., Murata, M., Li, W., Yuasa, S., Onizuka, T., Shimoji, K., Ohno, Y., Sasaki, E., Kimura, K., Hakuno, D., Sano, M., Makino, S., Ogawa, S., Fukuda, K., 2008. Common marmoset embryonic stem cell can differentiate into cardiomyocytes. Biochem. Biophys. Res. Commun. 369, 801–806.

Cheng, L., Hammond, H., Ye, Z., Zhan, X., Dravid, G., 2003. Human adult marrow cells support prolonged expansion of human embryonic stem cells in culture. Stem Cells 21, 131–142.

Choo, A., Padmanabhan, J., Chin, A., Fong, W.J., Oh, S.K., 2006. Immortalized feeders for the scale-up of human embryonic stem cells in feeder and feeder-free conditions. J. Biotechnol. 122, 130–141.

Choo, A., Ngo, A.S., Ding, V., Oh, S., Kiang, L.S., 2008. Autogeneic feeders for the culture of undifferentiated human embryonic stem cells in feeder and feeder-free conditions. Methods Cell Biol. 86, 15–28.

Hattori, F., Chen, H., Yamashita, H., Tohyama, S., Satoh, Y.S., Yuasa, S., Li, W., Yamakawa, H., Tanaka, T., Onitsuka, T., Shimoji, K., Ohno, Y., Egashira, T., Kaneda, R., Murata, M., Hidaka, K., Morisaki, T., Sasaki, E., Suzuki, T., Sano, M., Makino, S., Oikawa, S., Fukuda, K., 2010. Nongenetic method for purifying stem cell-derived cardiomyocytes. Nat. Methods 7, 61–66.

Hearn, J.P., 2001. Embryo implantation and embryonic stem cell development in primates. Reprod. Fertil. Dev. 13, 517–522.

Lee, J.B., Lee, J.E., Park, J.H., Kim, S.J., Kim, M.K., Roh, S.I., Yoon, H.S., 2005. Establishment and maintenance of human embryonic stem cell lines on human feeder cells derived from uterine endometrium under serum-free condition. Biol. Reprod. 72, 42–49.

Liu, H., Zhu, F., Yong, J., Zhang, P., Hou, P., Li, H., Jiang, W., Cai, J., Liu, M., Cui, K., Qu, X., Xiang, T., Lu, D., Chi, X., Gao, G., Ji, W., Ding, M., Deng, H., 2008. Generation of induced pluripotent stem cells from adult rhesus monkey fibroblasts. Cell Stem Cell 3, 587–590.

Lu, Y., Yang, S., 2009. Angiotensin II induces cardiomyocyte hypertrophy probably through histone deacetylases. Tohoku J. Exp. Med. 219, 17–23.

Nakatsuji, N., Suemori, H., 2002. Embryonic stem cell lines of nonhuman primates. ScientificWorldJournal 2, 1762–1773.

Olmer, R., Haase, A., Merkert, S., Cui, W., Palecek, J., Ran, C., Kirschning, A., Scheper, T., Glage, S., Miller, K., Curnow, E.C., Hayes, E.S., Martin, U., 2010. Long term expansion of undifferentiated human iPS and ES cells in suspension culture using a defined medium. Stem Cell Res. 5, 51–64.

Sasaki, E., Hanazawa, K., Kurita, R., Akatsuka, A., Yoshizaki, T., Ishii, H., Tanioka, Y., Ohnishi, Y., Suemizu, H., Sugawara, A., Tamaoki, N., Izawa, K., Nakazaki, Y., Hamada, H., Suemori, H., Asano, S., Nakatsuji, N., Okano, H., Tani, K., 2005. Establishment of novel embryonic stem cell lines derived from the common marmoset (*Callithrix jacchus*). Stem Cells 23, 1304–1313.

Sasaki, E., Suemizu, H., Shimada, A., Hanazawa, K., Oiwa, R., Kamioka, M., Tomioka, I., Sotomaru, Y., Hirakawa, R., Eto, T., Shiozawa, S., Maeda, T., Ito, M., Ito, R., Kito, C., Yagihashi, C., Kawai, K., Miyoshi, H., Tanioka, Y., Tamaoki, N., Habu, S., Okano, H., Nomura, T., 2009. Generation of transgenic non-human primates with germline transmission. Nature 459, 523–527.

Singh, H., Mok, P., Balakrishnan, T., Rahmat, S.N., Zweigerdt, R., 2010. Up-scaling single cell-inoculated suspension culture of human embryonic stem cells. Stem Cell Res. 4, 165–179.

Steiner, D., Khaner, H., Cohen, M., Even-Ram, S., Gil, Y., Itsykson, P., Turetsky, T., Idelson, M., Aizenman, E., Ram, R., Berman-Zaken, Y., Reubinoff, B., 2010. Derivation, propagation and controlled differentiation of human embryonic stem cells in suspension. Nat. Biotechnol. 28, 361–364.

Stojkovic, P., Lako, M., Stewart, R., Przyborski, S., Armstrong, L., Evans, J., Murdoch, A., Strachan, T., Stojkovic, M., 2005. An autogeneic feeder cell system that efficiently supports growth of undifferentiated human embryonic stem cells. Stem Cells 23, 306–314.

Takahashi, K., Yamanaka, S., 2006. Induction of pluripotent stem cells from mouse embryonic and adult fibroblast cultures by defined factors. Cell 126, 663–676.

Takahashi, K., Tanabe, K., Ohnuki, M., Narita, M., Ichisaka, T., Tomoda, K., Yamanaka, S., 2007. Induction of pluripotent stem cells from adult human fibroblasts by defined factors. Cell 131, 861–872.

Thomson, J.A., Itskovitz-Eldor, J., Shapiro, S.S., Waknitz, M.A., Swiergiel, J.J., Marshall, V.S., Jones, J.M., 1998. Embryonic stem cell lines derived from human blastocysts. Science 282, 1145–1147.

Tomioka, I., Maeda, T., Shimada, H., Kawai, K., Okada, Y., Igarashi, H., Oiwa, R., Iwasaki, T., Aoki, M., Kimura, T., Shiozawa, S., Shinohara, H., Suemizu, H., Sasaki, E., Okano, H., 2010. Generating induced pluripotent stem cells from common marmoset (*Callithrix jacchus*) fetal liver cells using defined factors, including Lin28. Genes Cells.

Unger, C., Gao, S., Cohen, M., Jaconi, M., Bergstrom, R., Holm, F., Galan, A., Sanchez, E., Irion, O., Dubuisson, J.B., Giry-Laterriere, M., Salmon, P., Simon, C., Hovatta, O., Feki, A., 2009. Immortalized human skin fibroblast feeder cells support growth and maintenance of both human embryonic and induced pluripotent stem cells. Hum. Reprod. 24, 2567–2581.

Wang, Q., Fang, Z.F., Jin, F., Lu, Y., Gai, H., Sheng, H.Z., 2005. Derivation and growing human embryonic stem cells on feeders derived from themselves. Stem Cells 23, 1221–1227.

Wu, Y., Zhang, Y., Mishra, A., Tardif, S.D., Hornsby, P.J., 2010. Generation of induced pluripotent stem cells from newborn marmoset skin fibroblasts. Stem Cell Res. 4, 180–188.

Xu, C., Inokuma, M.S., Denham, J., Golds, K., Kundu, P., Gold, J.D., Carpenter, M.K., 2001. Feeder-free growth of undifferentiated human embryonic stem cells. Nat. Biotechnol. 19, 971–974.

C-Reactive Protein Overexpression Exacerbates Pressure Overload–Induced Cardiac Remodeling Through Enhanced Inflammatory Response

Toshiyuki Nagai, Toshihisa Anzai, Hidehiro Kaneko, Yoshinori Mano, Atsushi Anzai, Yuichiro Maekawa, Toshiyuki Takahashi, Tomomi Meguro, Tsutomu Yoshikawa, Keiichi Fukuda

See Editorial Commentary, pp 151–153

Abstract—Serum C-reactive protein (CRP) elevation predicts the development of heart failure in patients with hypertension. CRP activates macrophages and enhances oxidative stress. We hypothesize that CRP itself has a pathogenic role in the development of pressure overload–induced cardiac remodeling. Transgenic mice with human CRP overexpression (CRPtg) and nontransgenic littermates (CON) were subjected to transverse aortic constriction (TAC/CRPtg and TAC/CON) or sham operation (Sham/CRPtg and Sham/CON). One week after operation, in TAC/CRPtg, myocardial mRNA levels of interleukin (IL)-6, CD68, glutathione peroxidase-3 (GPx3), 47-kDa α-subunit of nicotinamide adenine dinucleotide phosphate oxidase ($p47^{phox}$), and collagen-I, the number of infiltrating Mac-2–positive macrophages, nuclear localization of phosphorylated NF-κB/p65 (p-p65) in cardiomyocytes, nuclear NF-κB-DNA-binding activity, and reactive oxygen species (ROS) content were increased compared to those in TAC/CON. Cardiac fibrosis was more prominent in TAC/CRPtg compared to TAC/CON. Four weeks after operation, heart and lung weights, cardiomyocyte cross-sectional area, and the extent of cardiac fibrosis were greater in TAC/CON than in Sham/CON, and these differences were further augmented in TAC/CRPtg compared to TAC/CON. Left ventricular (LV) fractional shortening was less and LV end-diastolic pressure was higher in TAC/CRPtg than in TAC/CON. Myocardial mRNA levels of angiotensin type 1 receptor, atrial natriuretic factor, IL-6, GPx3, $p47^{phox}$, collagen-I, and transforming growth factor (TGF)-β1, the protein level of TGF-β1, and the numbers of Mac-2–positive macrophages and p-p65–positive cells were higher in TAC/CRPtg than in TAC/CON. In conclusion, CRP itself may have a pathogenic role in the development of pressure overload–induced cardiac remodeling, possibly through enhanced inflammation and oxidative stress. (***Hypertension.* 2011;57:208-215.) • Online Data Supplement**

Key Words: pressure overload ■ cardiac remodeling ■ C-reactive protein ■ inflammation ■ macrophage ■ NF-κB/p65

C-reactive protein (CRP), which is an acute-phase protein, has been regarded as a risk factor or biomarker for cardiovascular disease, including coronary artery disease, hypertension, and heart failure. Elevation of serum CRP is associated with left ventricular (LV) dysfunction and is a predictor of mortality and morbidity in patients with heart failure, independent of ischemic/nonischemic etiology and other established cardiovascular risk factors.[1–3] Laboratory evidence suggests that CRP not only serves as a biomarker but also upregulates the angiotensin type 1 receptor (AT_1R),[4] stimulates proinflammatory cytokine production,[5] and attenuates nitric oxide (NO) production.[6] In addition, pathological examination of endomyocardial biopsies in patients with dilated cardiomyopathy revealed that CRP is frequently present in the myocardium and colocalizes with complement and macrophages.[7] Furthermore, CRP is reported to promote fibrosis and inflammation in angiotensin II-induced cardiac remodeling.[8] These findings suggest that CRP itself may play some role in the development of LV dysfunction and remodeling.

Human CRP is mainly produced in the liver in response to infection, acute injury, or other inflammatory stimuli. Although CRP is not an acute-phase reactant in mice and is minimally expressed, human CRP can activate complement (A, B, and C) in mice[9] and bind to mouse Fcγ receptor I (FcγRI) and FcγRIIb, which provoke inflammation and oxidative stress.[10] Therefore, transgenic mice carrying the human CRP gene provide a viable model to investigate the role of CRP in vivo.[9]

We investigated the role of CRP in pressure overload–induced cardiac remodeling, especially its effect on inflamma-

Received July 12, 2010; first decision August 7, 2010; revision accepted November 30, 2010.
From the Division of Cardiology, Department of Medicine, Keio University School of Medicine, Tokyo, Japan.
Correspondence to Toshihisa Anzai, 35 Shinanomachi, Shinjuku-ku, Tokyo 160-8582, Japan. E-mail anzai@cpnet.med.keio.ac.jp

Hypertension is available at http://hyper.ahajournals.org DOI: 10.1161/HYPERTENSIONAHA.110.158915

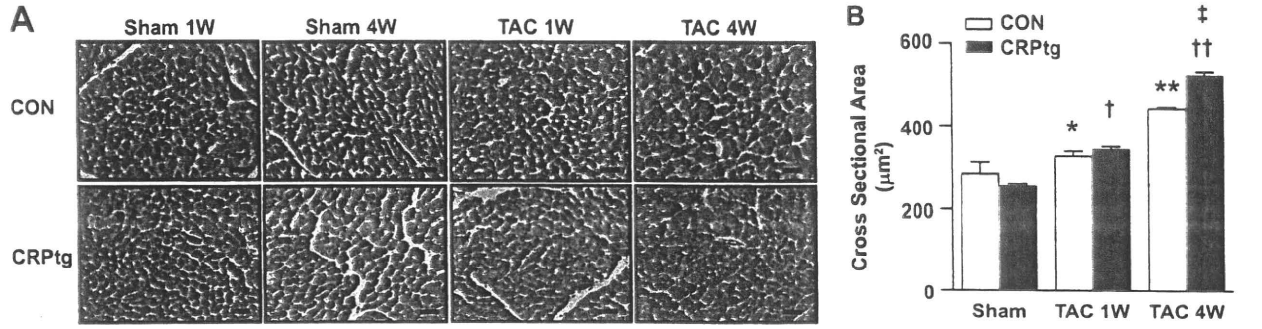

Figure 1. Pressure overload–induced cardiac hypertrophy. A, Hematoxylin-eosin staining of ventricular tissue. Bars=30 μm. B, CSA of ventricular cardiomyocytes in the LV tissue of CRPtg and control mice 1 and 4 weeks after TAC or sham operation. *P<0.05, **P<0.01 vs Sham/CON; †P<0.05, ††P<0.01 vs Sham/CRPtg; ‡P<0.01 vs TAC/CON. 1W indicates 1 week; 4W, 4 weeks.

tion and oxidative stress, using human CRP-overexpressing transgenic (CRPtg) mice.

Materials and Methods

A detailed Methods section can be found in the online Data Supplement (available at http://hyper.ahajournals.org).

Experimental Animals

CRPtg mice (C57BL/6 background) were generated under the control of the CAG promoter to induce ubiquitous transgene expression as described previously.[11] Male CRPtg (9 to 12 weeks of age) and their age-matched male nontransgenic littermates (CON) were used.

Mouse Model of Transverse Aortic Constriction and Experimental Study Protocol

Twenty-eight CRPtg and 28 CON underwent transverse aortic constriction (TAC) operation. The TAC procedure was reported in a previous study,[12] as described in the online Data Supplement Methods section. Mice were euthanized 1 and 4 weeks after TAC or sham operation. Cardiac tissue was collected for gene expression quantification, protein analysis, and histological examination.

Additional Methods

The expanded Methods section in the Online Data Supplement contains information on the hemodynamic measurements, echocardiographic analyses, immunoblotting, tissue analyses, immunohistochemical staining, dihydroethidium (DHE) staining, electrophoretic mobility shift assay (EMSA), measurement of serum CRP, measurement of CRP, tumor necrosis factor (TNF)-α, NO, inducible NO synthase (iNOS) in cardiac tissue, and quantification of gene expression by real-time polymerase chain reaction (RT-PCR).

Statistical Analysis

All continuous data were expressed as mean±SEM. The statistical significance of differences between multiple groups was determined using one-way ANOVA and post hoc analysis with the Bonferroni test. A probability value of <0.05 was considered to be significant. All statistical analyses were performed using the SPSS 15.0 statistical software package for Windows (SPSS Inc.).

Results

CRPtg Mice

Gene expression in the heart was confirmed by RT-PCR with primers for human CRP (Figure S1A). Protein expression in the heart was also confirmed by immunoblotting of LV homogenates with antibodies recognizing human CRP (Figure S1B) and immunohistochemical staining (Figure S1C and S1D).

Body and Organ Weights, CRP Levels, and Cardiac Function

The body, heart, lung weights, and serum and cardiac CRP levels are summarized in Table S1. Mice with TAC operation showed increased heart weight 1 week after operation, compared to that in sham-operated mice, but there was no difference between TAC/CRPtg and TAC/CON. Four weeks after TAC operation, the weights of the heart and lungs were further increased compared to those in sham-operated mice, and these parameters, lung weight/body weight ratio and lung wet/dry ratio in TAC/CRPtg, were significantly higher than those in TAC/CON. Both serum and cardiac CRP levels in CRPtg were significantly increased compared to those in CON; however, no difference was noted between CRPtg with and without TAC operation.

The echocardiographic data are shown in Table S2. One week after operation, there were no significant differences in echocardiographic parameters among the four groups. Four weeks after operation, LV dimensions and wall thickness were greater and LV fractional shortening and velocity of circumferential fiber shortening were smaller in TAC-operated mice compared to their sham-operated counterparts. These changes were further augmented in TAC/CRPtg compared to TAC/CON.

Hemodynamic data are shown in Table S3. Right carotid systolic arterial pressure and LV systolic pressure 1 and 4 weeks after TAC operation were increased compared to those in sham-operated mice. Pressure gradient across the aortic constriction 1 and 4 weeks after TAC operation was comparable between TAC/CRPtg and TAC/CON. LV end-diastolic pressure 4 weeks after TAC operation was significantly higher in TAC/CRPtg than in TAC/CON.

Cardiac Hypertrophy and Fibrosis

Hematoxylin-eosin staining of the heart showed that cardiomyocyte cross-sectional area (CSA) was greater in TAC/CON than in Sham/CON 1 and 4 weeks after operation. The increase in CSA was further augmented in TAC/CRPtg compared with TAC/CON 4 weeks after operation (Figure 1). Triphenyltetrazolium chloride (TTC) staining 1 and 4 weeks after TAC operation showed that there was no TTC-positive area in TAC/CRPtg and TAC/CON.

Staining with Masson's trichrome showed cardiac fibrosis in both the interstitial and perivascular areas 1 week after

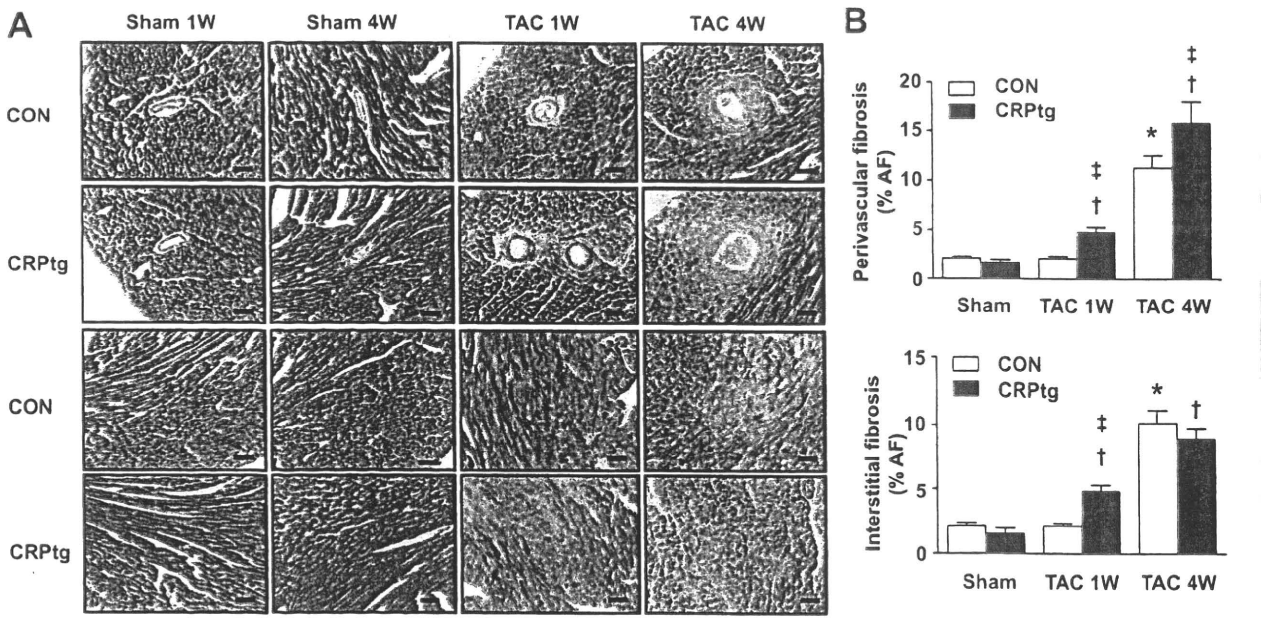

Figure 2. Pressure overload–induced cardiac fibrosis. A, Masson's trichrome staining of perivascular and interstitial ventricular tissue. Bars=50 μm. B, Relative amount of fibrotic tissue (% AF) in the perivascular and interstitial ventricular tissue of CRPtg and control mice 1 and 4 weeks after TAC or sham operation. *$P<0.05$ vs Sham/CON; †$P<0.05$ vs Sham/CRPtg; ‡$P<0.05$ vs TAC/CON. 1W indicates 1 week; 4W, 4 weeks.

TAC operation (Figure 2). There was a significantly increased percentage of area fraction in both the interstitial and perivascular areas of the LV in TAC/CRPtg compared to TAC/CON. Four weeks after operation, the percentage of area fraction in the perivascular area of the LV was markedly higher in TAC/CRPtg than in TAC/CON, although there was no significant difference in the interstitial area between TAC/CRPtg and TAC/CON (Figure 2).

Myocardial Expression of Hypertrophic and Fibrotic Markers

Myocardial mRNA expression of atrial natriuretic factor (ANF) in TAC/CRPtg was increased 1 and 4 weeks after operation compared to that in Sham/CON. ANF expression in TAC/CRPtg 4 weeks after operation was significantly higher than that in TAC/CON (Figure 3A). Myocardial mRNA expression of B-type natriuretic peptide 4 weeks after operation was higher in TAC/CRPtg than in Sham/CRPtg or TAC/CON (Figure 3B). Myocardial mRNA expression of collagen-I and transforming growth factor (TGF)-β1 1 and 4 weeks after operation was significantly higher in TAC/CRPtg than in TAC/CON or sham-operated mice (Figure 3C and 3E). Myocardial connective tissue growth factor mRNA level 4 weeks after operation was higher in TAC/CRPtg than in TAC/CON or sham-operated mice (Figure 3D). Myocardial protein expression of TGF-β1 in TAC/CON 4 weeks after operation was increased compared to that in Sham/CON. Its level was higher in TAC/CRPtg than in TAC/CON (Figure 3F).

Inflammatory Cytokines, Oxidative Stress, and Renin-Angiotensin System

Expression of interleukin (IL)-6 mRNA in myocardial tissue of TAC/CRPtg was markedly elevated compared to that in Sham/CRPtg or TAC/CON, peaking 1 week after operation. Its expression was persistently elevated in TAC/CRPtg 4 weeks after operation compared to that in Sham/CRPtg or TAC/CON (Figure 4A). In contrast, the level of TNF-α mRNA showed little change in either TAC/CON or TAC/CRPtg 1 week after operation but was significantly higher in TAC/CRPtg than in either Sham/CRPtg or TAC/CON 4 weeks after operation (Figure 4A). Furthermore, the protein expression of TNF-α was higher in TAC/CRPtg compared to TAC/CON at 4 weeks after TAC operation (Figure 4B).

The oxidative stress markers glutathione peroxidase-3 (GPx3) and 47-kDa α-subunit of nicotinamide adenine dinucleotide phosphate oxidase ($p47^{phox}$) showed a similar expression pattern to that of IL-6. Myocardial mRNA levels of both factors were significantly elevated in TAC/CRPtg compared to those in either TAC/CON or sham-operated mice 1 week after operation, and these differences remained 4 weeks after operation (Figure 4C). DHE staining showed that reactive oxygen species (ROS) content was greater in TAC/CRPtg than in TAC/CON at 1 week after TAC operation (Figure 4D).

Expression of both angiotensinogen and AT_1R mRNA in myocardial tissue was significantly higher in both TAC/CRPtg and TAC/CON compared to that in their sham-operated counterparts. One week after operation, myocardial mRNA expression of both factors was comparable between TAC/CRPtg and TAC/CON. However, 4 weeks after operation, it was significantly higher in TAC/CRPtg than in TAC/CON (Figure 4E).

p38 Mitogen-Activated Protein Kinase Signaling and NO Production

Myocardial protein expression of phosphorylated p38 mitogen-activated protein kinase (MAPK; p-p38) was ele-